Importance of Dynamic Effects in Isobutanol to Linear Butenes Conversion Catalyzed by Acid Zeolites Assessed by AIMD

Monika Gešvandtnerová, Pascal Raybaud, Céline Chizallet, Tomáš Bučko

Importance of dynamic effects in isobutanol to linear butenes conversion catalyzed by acid zeolites assessed by AIMD

Monika Gešvandtnerová,[†] Pascal Raybaud,[‡] Céline Chizallet,[*,‡] and Tomáš Bučko[*,†,¶]

†*Department of Physical and Theoretical Chemistry, Faculty of Natural Sciences, Comenius University in Bratislava, Mlynská Dolina, SK-84215 Bratislava, SLOVAKIA*

‡*IFP Energies nouvelles, Rond-Point de l'échangeur de Solaize, BP3, 69360 Solaize, FRANCE*

¶*Institute of Inorganic Chemistry, Slovak Academy of Sciences, Dúbravska cesta 9, SK-84236 Bratislava, SLOVAKIA*

E-mail: celine.chizallet@ifpen.fr; tomas.bucko@uniba.sk

Abstract

Dehydration of alcohols into alkenes is a key-reaction for the production of fuels and chemicals from biomass. However, the mechanism of these reactions is highly questionable, hindering the rational optimization of efficient catalysts. In the present work, the formation of linear butenes starting from isobutanol catalyzed by proton exchanged-zeolites is unraveled by *ab initio* molecular dynamics (AIMD). Comparison with static calculations done for a gas phase reaction catalyzed by a proton, and for the prototypical chabazite zeolite framework, shows that AIMD estimations of the free energy barriers are significantly different from the static ones. Moreover, a common transition state is found for two competing reactions, namely the isomerization of

isobutanol into butan-2-ol (the dehydration of the later yielding linear butenes), and the synchronous dehydration and isomerization of isobutanol into products related to linear butenes in a single step. The existence of a post-transition state bifurcation prevents a traditional estimation of rates by the transition state theory. To circumvent this problem, we quantify relative transmission coefficients using the Bennett-Chandler theory, which shows a clear tendency for decrease of relative frequency for isobutanol isomerization and increase of that for synchronous dehydration and isomerization when switching from 100 to 500 K. This work represents a step forward for the accurate determination of rates for key reactions in alcohol dehydration reactions.

Keywords

acidic zeolites, dehydration, isomerization, ab initio molecular dynamics, biobutanol, ,

1 Introduction

The catalytic transformations of oxygenates play a prominent role in the current transition from fossil to renewable sources for the production of fuels and chemicals. One of the reactions highly debated in the context of green chemistry is transformation of isobutanol available from biomass,[1] into linear and branched butenes[2,3] used as reactive precursors for the production of longer hydrocarbon chains for further industrial processing.[4] While the reaction can be catalyzed by different zeolites, very different results in terms of conversion and selectivity towards linear products (with respect to isobutene) are observed as a function of the zeolite topology and of operating conditions,[2,3,5] for reasons that are not elucidated yet. Moreover, the linear versus branched alkenes selectivity is contrasting with results obtained in butene isomerization reactions.[6–9]

Thus, despite high technological potential, the mechanisms of these transformations are not yet fully understood, in particular those leading to linear butenes from isobu-

tanol.[10] Our previous theoretical work[11] represents the first systematic effort to explore possible transformation routes linking isobutanol to all main products, including isobutene, but-1-ene, and cis- and trans-but-2-ene. In addition to the conventional dehydration mechanism proceeding via alkoxide intermediates, known also from previous literature reports on linear alcohol transformation,[12–15] we revealed an as yet unexplored mechanism involving isobutanol isomerization into butan-2-ol (path I2 in Figure 1) followed by the dehydration of the later into linear butenes, including but-1-ene (DH4 elementary step in Figure 1). The I2 isomerization reaction was shown to pass through a transition state in which the protonated OH moiety (thus becoming a labile water molecule) exchanges its position with a methyl group, whereas the DH4 dehydration step follows a E2 mechanism, with synchronous C-O and C-H bond breakings. We also discovered a surprising new reaction mechanism in which the isomerization and dehydration are combined into a single reaction step (path DHI in Figure 1). In this case, the leaving water molecule deprotonates the close-by C-H bond, while a methyl group shifts. Importantly, our analysis based on static DFT calculations combined with the energy span concept[16,17] suggests that the I2+DH4 combination dominates over DHI at relevant experimental conditions, with differences in their respective free energy spans being as large as 16 kJ mol^{-1}. Given the approximations made, however, it is mandatory to revise this result using more rigorous approach.

The main objective of our previous work was to identify the relevant reaction mechanisms. We pragmatically used static approach based on relaxations and vibrational analysis of stationary states. However, in H-exchanged zeolites, the proton is transferred to the reactant molecule, leading to charged species which then exhibit significant mobility that is not taken into account in static approaches. In reference ,[18] for instance, the case of C7 alkene isomerization (proceeding through carbenium intermediates) in the chabazite framework was investigated. It was shown that a large set of local energy minima could be identified for reactants and products by static approaches, with a typical variation in

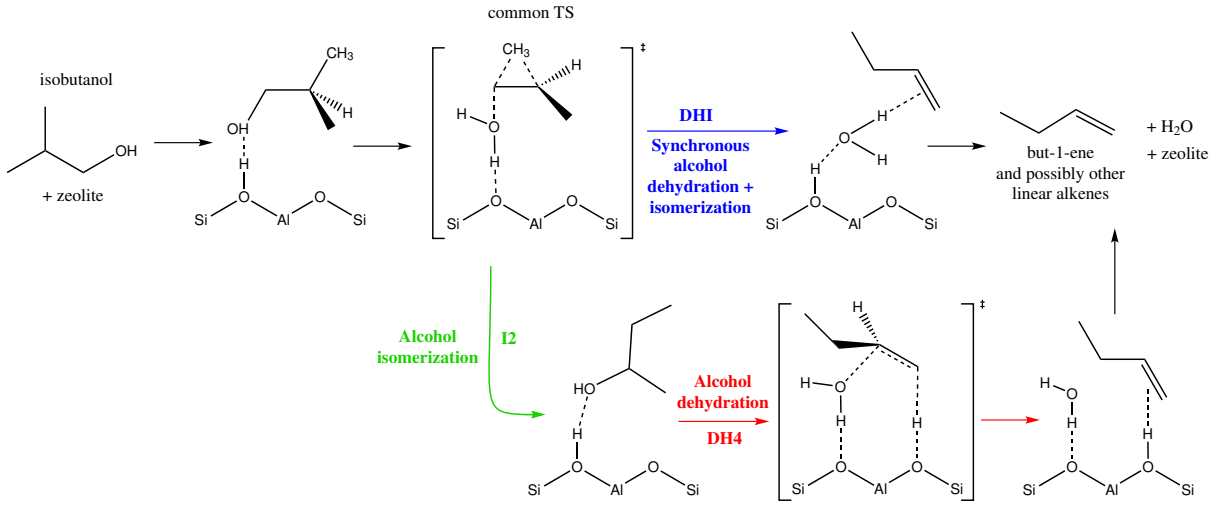

Figure 1: Reaction network of monomolecular isobutanol transformations into but-1-ene, and possibly other linear alkenes, either through a synchronized dehydration and isomerization step (DHI, following the terminology introduced in ref[11]) or an isomerization step (I2) into butan-2-ol followed by its dehydration (DH4).

free energies of 20 kJ mol^{-1}, and an even broader distribution of free energies (about 40 kJ mol^{-1}) was found for a set of optimized transition states. This led to unreliable barrier determinations ranging between ∼30 to ∼100 kJ mol^{-1} at 300 K. The main difference between the configurations optimized was the relative location of the charged species with respect to the aluminum atom in the zeolite framework. Similar observations were reported in reference [19] for the cracking of propane. Even larger variations in the activation barrier (almost 80 kJ mol^{-1} at 773 K) were observed by Cnudde et al.[20] who compared several conformations for the cracking of a C8 carbenium ion in ZSM-5.

This problem can be tackled[18–23] by using some of the *ab initio* molecular dynamics (AIMD) techniques designed to treat rare events, such as metadynamics,[24] umbrella sampling,[25] or bluemoon ensemble approach.[26,27] Regardless of the particular method of choice, the computational cost of such simulations is several orders of magnitude higher compared to the static approach, since *ab initio* calculations need to be performed for at least a few hundreds of thousands structures generated in order to achieve a reasonable convergence for all degrees of freedom of the system, including the slowest ones. To

give a few illustrative examples of importance of the AIMD methods in catalytic applications, let us mention the work of Cnudde et al.[28] who showed that the stability ranking of adsorbed alkenes, carbenium ions and alkoxides changed completely when static calculations were replaced by metadynamics, demonstrating that the former approach is not reliable in identification of the kinetically relevant intermediates. Furthermore, the AIMD result for the free energy of activation for the C7 alkene isomerization[18] ($\sim$70 kJ mol^{-1}) was found to fall in the middle of the broad interval of values ($\sim$30 to $\sim$100 kJ mol^{-1}) predicted in the static approach, from which it is clear that not only the magnitude, but also the sign of the error of the static approach can strongly depend on the choice of the particular configurations used in relaxations, and such large variations can occur even within the same chemical reaction. More recently, by using AIMD and the Hill relation,[29] Pigeon et al. quantified directly (i.e. circumventing thermodynamic integration) various reaction constants for water rotation and dissociation on an oxide surface.[30] In this case, their study revealed that such reaction constants could be underestimated by up to 2 orders of magnitude by static harmonic TST approach with respect to AIMD-Hill approach. The reactions discussed in the present work (isobutanol isomerization and dehydration) are catalyzed by proton exchanged zeolites, and the species involved (intermediates / transition states) are detached from the zeolite framework and can be expected to exhibit a high mobility. But since, to the best of our knowledge, these reactions have never been investigated by AIMD, it is important to obtain information about the relevance of the mechanisms which we previously proposed by static approaches, and to quantify the impact of anharmonic and dynamical effects on free energy barriers.

In this work, we use Blue moon ensemble AIMD[26,27] in combination with Bennett-Chandler theory[31,32] and Transition Path Sampling[33] (TPS) to study the two key reaction mechanisms of isobutanol to butenes transformations identified in our previous study.[11] Namely, we compare a two step mechanism consisting of isobutanol isomerization into butan-2-ol(labeled as I2) followed by conversion of the latter into but-1-ene (denoted

DH4), with the generalization of the competing reaction DHI, in which isomerization and dehydration occur as a single reaction step, see Figure 1. Notably, the synchronous isomerization and dehydration will be called DHI (instead of DHI2 used in our previous work[11] for the specific case of DHI reaction leading to formation of but-1-ene) in what follows, because of the variety of linear products obtained in the present AIMD investigation. We will show that going beyond the static approach reveals very important features of these two reactions, in particular the existence of a common transition state that prevents the application of transition state theory to deduce respective rates. Consideration of dynamical effects via transmission coefficients is thus needed to quantify the relative frequency of the two reactions in the production of linear butenes. Reactions with common transition states and post-transition state bifurcations are known from the literature[34–39] in organic chemistry and biochemistry. The present work is probably the first report of post-transition state bifurcation for a complex catalytic reaction occurring at the surface of a heterogeneous catalyst.

In this work, in order to understand better the nature of the transformation, a gas phase variant of the isobutanol to butan-2-ol isomerization and its subsequent dehydration are discussed first. Next, we show how the entropy effect stabilizes carbenium ion (precursor of linear alkenes) as an alternative product to the protonated linear alcohol. Making use of the information on the gas phase variants of the I2+DH4 and DHI reactions, various roles of the zeolite framework in these transformations are then identified. Most importantly, our results suggest the existence of a post-transition state bifurcation for these two reactions, which prevents the use of transition state theory to deduce respective rates. Hence, we compute transmission coefficients, to identify the preferred reaction pathway. The conclusions made strongly differ with respect to previous static estimates and bring important new insights in the relevant mechanisms explaining the formation of linear butenes from isobutanol.

2 Simulation details

2.1 Electronic structure calculations

Periodic DFT calculations were performed using the VASP code.[40–42] The Kohn-Sham equations have been solved variationally in a plane-wave basis set using the projector-augmented-wave (PAW) method of Blöchl,[43] as adapted by Kresse and Joubert.[44] The PBE exchange-correlation functional in the generalized gradient approximation proposed by Perdew et al.[45] was used. The D2 correction of Grimme[46] as implemented in VASP[47] was applied to account for long-range dispersion interactions. Plane wave cutoff energy was set to 400 eV, and the convergence criterion for the SCF cycle was set to 10^{-6} eV/cell. Owing to the relatively large unit cell used in our simulations, the Brillouin zone sampling was restricted to the Γ-point. The atomic charges have been computed using the iterative Hirshfeld (HI) partitioning,[48] as implemented in VASP.[49] The structural model of chabazite (CHA) used in previous theoretical works of Rey et al.[18] and Gešvandtnerová et al.[11] has been employed. This model contains 24 tetrahedral sites and one bridging OH group site created by one of the Si framework atoms being replaced by an Al atom and one hydrogen atom placed at the O1 position (Figure S1 in the Supporting Information). We note that this OH group belongs to highly populated Brønsted acid (BA) sites of CHA.[50]

2.2 Molecular dynamics simulations and free energy calculations

Born-Oppenheimer *ab initio* molecular dynamics (AIMD) simulations were performed in the NVT ensemble. In the calculations aimed at determination of ensemble averages, temperature was maintained by Andersen thermostat[51] with the frequency of stochastic collisions set to 0.01 fs^{-1} per atom. For the simulations of the transition state (TS) crossing trajectories the use stochastic thermostat is less suitable in practice as it slows down the convergence. For this reason, we used in this type of simulations, and in the

transition path sampling (TPS) simulations, a deterministic Nose-Hoover thermostat[52,53] with mass-like parameter automatically adjusted such that the characteristic period of the thermostat was approximately 40 time steps. In all cases, integration of classical equations of motion was realized via leapfrog Verlet algorithm[54] with an integration step of 1 fs, whereby mass of tritium was used for hydrogen atoms. The equilibration period was chosen for each point on free energy profile separately so that the data corresponding to the production period were trend free, as tested by the Mann Kendall test for average and variance[55] (see Section SII of Supporting Information).

For a given reaction coordinate ξ, the reversible work $\Delta A_{ref,R\to\xi^*}$ needed to shift the reaction coordinate from the value corresponding to an arbitrarily chosen reactant reference state ($\xi_{ref,R}$) to free energy transition state (ξ^*) occuring in expression for Helmholtz free energy of activation:[26,56]

$$\Delta A^{\ddagger}_{R\to P} = \Delta A_{\xi_{ref,R}\to\xi^*} - k_B T \ln\left\{\frac{h}{k_B T}\frac{\langle|\dot{\xi}^*(0)|\rangle}{2}P(\xi_{ref,R})\right\} \tag{1}$$

is calculated by Blue moon ensemble method.[26,27] The generalized velocity term[27] for time t=0:

$$\langle|\dot{\xi}^*(0)|\rangle = \sqrt{\frac{2k_B T}{\pi}}\frac{1}{\langle Z^{-1/2}\rangle_{\xi^*}} \tag{2}$$

is calculated from $Z = \sum_{i=1}^{N}\sum_{\nu=x,y,z}\frac{1}{m_i}\left(\frac{\partial\xi}{\partial q_{i,\nu}}\right)^2$, where N is the number of atoms and $\boldsymbol{q}_i$, m_i is the Cartesian coordinates and mass of an atom i, and $\langle\cdots\rangle_{\xi^*}$ is the constrained NVT ensemble average with ξ fixed at ξ^*. Finally, the probability density term $P(\xi_{ref,R}) = \langle\delta(\xi_{ref,R} - \xi(\boldsymbol{q}))\rangle$ is determined from an unconstrained MD of reactant via histogram approximation.

Combining eq 1 for the forward and reverse reaction mode, the formula for free energy of reaction ($\Delta A_{R\to P}$) can be derived:[57]

$$\Delta A_{R\to P} = \Delta A_{\xi_{ref,R}\to\xi_{ref,P}} - k_B T \ln\left\{\frac{P(\xi_{ref,R})}{P(\xi_{ref,P}}\right\}, \tag{3}$$

where $\xi_{ref,P}$ is an arbitrarily chosen product reference state.

In this work, the path-based coordinate s introduced by Branduardi et al.[58] is used as a reaction coordinate ξ. The coordinate is defined as:

$$s(\boldsymbol{q}) = \frac{1}{M-1} \frac{\sum_{i=1}^{M} (i-1) \exp\left[-\lambda (\boldsymbol{\chi}(\boldsymbol{q}) - \tilde{\boldsymbol{\chi}}_i))^2\right]}{\sum_{i=1}^{M} \exp\left[-\lambda \left(\boldsymbol{\chi}(\boldsymbol{q}) - \tilde{\boldsymbol{\chi}}_i\right)^2\right]}, \tag{4}$$

where M is the number of approximately equidistant points $\tilde{\boldsymbol{\chi}}_i$ of discretized intrinsic reaction coordinate (IRC) expressed in terms of r internal coordinates $\chi_k(\boldsymbol{q})$ that are involved in the reaction of interest, $\boldsymbol{\chi}(\boldsymbol{q})$ is a vector $\boldsymbol{\chi}(\boldsymbol{q}) = \{\chi_k(\boldsymbol{q}); k = 1, \ldots, r\}$, and λ is an adjustable parameter. Following ref,[58] the value of λ is chosen to correspond to the inverse squared distance between two neighbouring points $\tilde{\chi}(i)$. The IRCs needed to define s were obtained using damped velocity Verlet algorithm.[59] The particular choice of basis function $\boldsymbol{\chi}(\boldsymbol{q})$ and the IRC parametrization is provided in Section SII of the Supporting Information.

By design, the coordinate s measures progress of the process defined by the IRC and varies between values 0 and 1. For practical reasons, it is also useful to define a complementary coordinate:

$$z(\boldsymbol{q}) = -\frac{1}{\lambda} \ln \sum_{i=1}^{M} \exp\left[-\lambda \left(\boldsymbol{\chi}(\boldsymbol{q}) - \tilde{\boldsymbol{\chi}}_i\right)^2\right], \tag{5}$$

measuring the 'distance' of the structure $\boldsymbol{q}$ from the IRC. In the $M \to \infty$ limit, z takes values from the interval (0,∞). However, when M is finite, as it is always the case in practice, z can take also small negative values. In this work we use z as a convenient tool to avoid by-reactions. In particular, a Fermi-type bias potential of the form:

$$W(z) = \frac{A}{1 + \exp\left\{-D\left(\frac{z(\boldsymbol{q})}{z_0} - 1\right)\right\}} \tag{6}$$

is applied on z with the parameters z_0, D, and A set to 0.2, 5, and 5, respectively. This

setting ensures that the sampling is restricted to the configuration space with $z \lesssim 0.1$ corresponding to the regions relatively close to the IRC. The effect of restraint is then eliminated by applying free energy perturbation theory.[60] To this end, an unbiased free energy (A) is obtained from the biased one ($\tilde{A}$) as follows:

$$A = \tilde{A} - k_B T \ln \langle e^{W/k_B T} \rangle_{\tilde{H}}. \tag{7}$$

where $\tilde{H} = H + W$ and H are the Hamiltonians of restricted and unrestricted systems, respectively. Free energy perturbation theory combined with eq 1 yields the following expression for the unbiased free energy of activation:[61]

$$\Delta A^{\ddagger}_{R \to P} = \Delta \tilde{A}^{\ddagger}_{R \to P} - k_B T \ln \left\{ \frac{\langle e^{W/k_B T} \rangle_{\xi^*}}{\langle e^{W/k_B T} \rangle} \right\}, \tag{8}$$

from which it is clear that corrections need to be applied only to the free reactant and the constrained transition state configurations, but not to any intermediate point used in thermodynamic integration.

The transmission coefficients (κ) were computed using the Bennett-Chandler theory[31,32] as follows:

$$\kappa = \frac{\langle \dot{\xi}(0) \theta \left(\xi^* - \xi(-t) \right) \theta \left(\xi(t) - \xi^* \right) \rangle_{\xi^*}}{\langle \dot{\xi}(0) \theta \left(\dot{\xi}(0) \right) \rangle_{\xi^*}}, \tag{9}$$

where $\xi(t)$ is the value of ξ at the time t and $\theta(x)$ is the Heaviside step function.

3 Results

3.1 I2 and DH4 reactions in the gas phase

We start our analysis by considering the gas phase variant of the isobutanol transformation into butan-2-ol (isomerization I2, Figure 1), which is the simplest realization of this transformation. Since the I2 reaction in zeolite is catalyzed by a Brønsted acid site with

protonation of the OH group being the first reaction step, we consider here the cationic form of all intermediates with the stoichiometry $(C_4H_{11}O)^+$. In the course of reaction, the CH and CH_2 groups exchange the CH_3 group (labeled in Figure 2 as 1, 2, and 3, respectively), initially located on CH, and the H_2O group, initially located on CH_2. In the course of the CH_3 exchange, the lengths of the original and the newly formed C-C bonds anticorrelate, i.e., while one increases, the other decreases, see Figure 3. The way the H_2O is exchanged is qualitatively different from CH_3 exchange in that both the C-O distances involved initially increase. At one point occurring after crossing TS, the nearest C-O distance is ∼2.9 Å and 96 % of the charge is localised at the C_4H_9 fragment, thus exhibiting carbenium nature, while water molecule is almost neutral (see Figure 4). The orientation of the H_2O molecule and its position with respect to the carbenium do not seem to indicate any significant specific interactions between these two fragments. The fact that virtually independent water molecule and carbenium cation are created during the I2 reaction can be documented also by a close similarity of the structure of free cation relaxed without water and one of the structures lying on the IRC after crossing TS, see Figure S20. As we shall see, this detachment of H_2O has important consequences for thermally induced modifications of reaction mechanism.

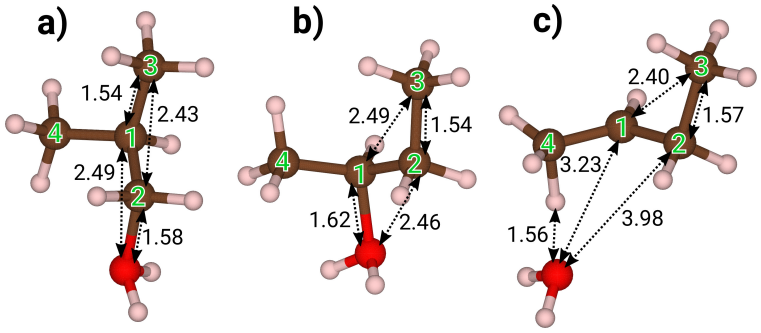

Figure 2: Relaxed structures of reactant of I2 and DHI (a), product of I2 and reactant of DH4 (b) and product of DH4 and DHI (c) reactions of protonated isobutanol in the gas phase. Selected interatomic distances are given in Å. Color code: C in brown, O in red, H in white. Numbering of C atoms is used within the text to describe reaction mechanisms.

Geometries of relaxed reactant, product and transition states are shown in Figure 2

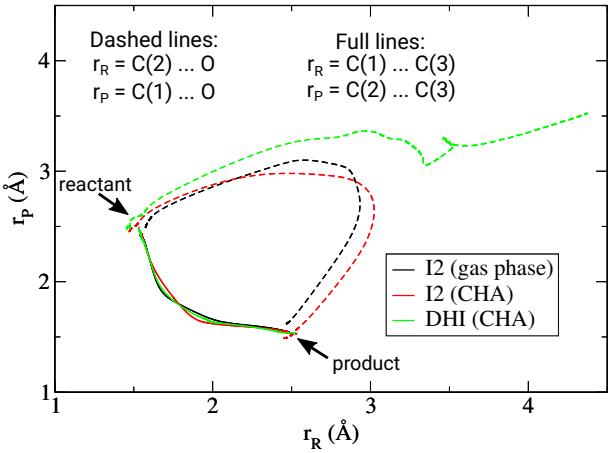

Figure 3: Correlations of pairs of C$\cdots$C (full lines) and O$\cdots$C (dashed lines) distances, measured along the IRC, involved in the I2 and DHI transformations in gas phase and in acid chabazite (CHA). Symbols r_R and r_P stand for distances between atomic pairs that form bonds in reactant and product, respectively. Numbering of atoms correspond to Figure 2.

and 5, while the thermodynamic properties computed for three different temperatures are compiled in Table 1. According to the static approach, free energy of activation decreases from 43.5 kJ mol^{-1} at 100 K to only 20.9 kJ mol^{-1} at 500 K. The internal energy of activation, on the other hand, decreases only moderately over the same temperature interval (from 50.0 to 46.7 kJ mol^{-1}). Hence, the large decrease of $\Delta A^{\ddagger}$ is mostly an entropic effect caused by a relative stabilization of transition state with respect to reactant. This stabilization can be explained by the fact that the H_2O molecule in TS is, unlike in the reactant, fully detached from the hydrocarbon torso (the shortest interatomic distance between H_2O and $(C_4H_9)^+$ is 2.49 Å, see Figure 5), gaining thus in entropy via significant softening of the corresponding vibrational degrees, now representing hindered rotations and translations.

In contrast, the reaction free energies are largely insensitive to temperature changes. This is not surprising because both the reactant and the product are very similar in terms of the number and type of bonds. Consequently, the differences in vibrational entropies are virtually negligible (see Table 1) and the free energy of reaction predicted by the static

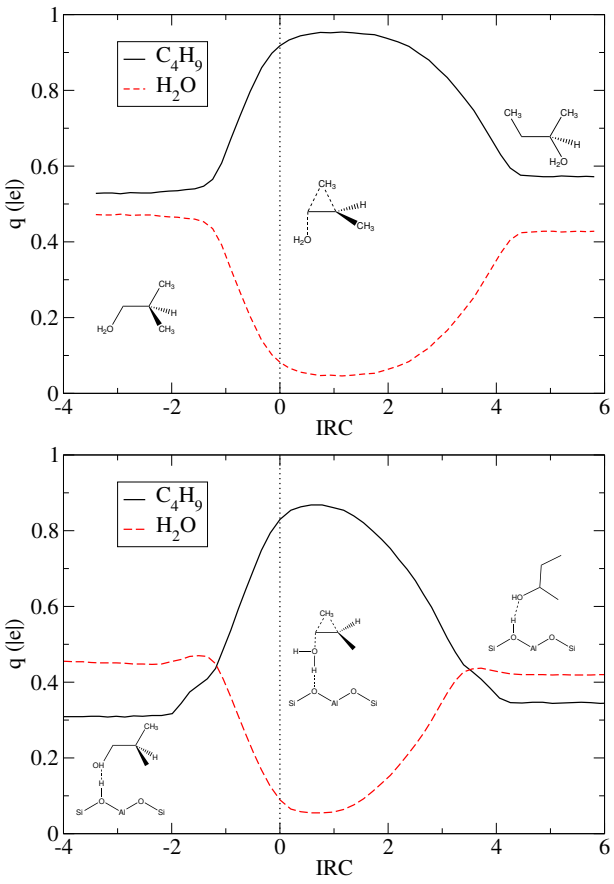

Figure 4: Change of charges localized on the C_4H_9 and H_2O fragments during the I2 reaction of isobutanol as a function of IRC. Results for the transformation in the gas phase (above) and in CHA (below) are shown. Dotted line indicates the position of TS.Note that in the gas phase reaction, the whole system holds a +1 charge.

approach is given almost entirely by the difference in electronic energies of relaxed reactant and product configurations.

The nature of TS prompts the question to what extent the naive static approach is appropriate for calculations of free energy of the I2 reaction. In particular, since its H_2O and $(C_4H_9)^+$ fragments seem to be only loosely interacting, the degrees of freedom that describe their relative position and orientation are likely to be of a non-vibrational character. To explore this problem, we performed AIMD free energy calculations as described in Section 2.2. Free energy profiles obtained by Blue moon ensemble approach are shown in Figure 6. As it follows from the numerical results shown in Table 1, the activation free

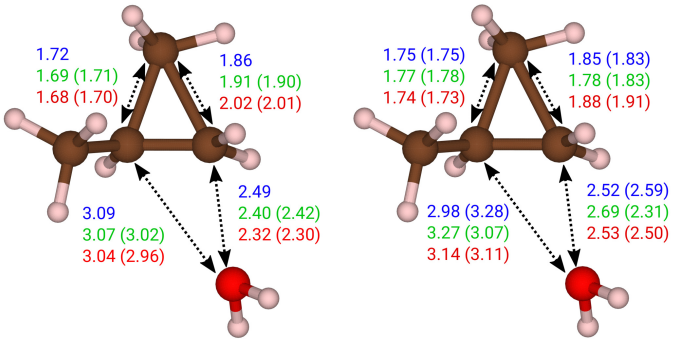

Figure 5: Selected interatomic distances (Å) in TS configurations of the I2 and DHI (values in parentheses) reactions in the gas phase (left) and in acid chabazite (right) at three different T: 0 K (blue), 100 K (green) and 500 K (red). Note that the 0 K results correspond to the geometries of relaxed structures, whereas the finite T data were obtained as averages of from AIMD simulations of dynamical TS structures.

energies obtained from AIMD are systematically higher compared to those determined via the static approach, which is most likely a consequence of overestimating entropy of transition state by the static approach. At 100 K, this difference is only 4.4 kJ mol^{-1}, which constitutes ∼10 % of the $\Delta A^{\ddagger}$ computed. As expected, the difference becomes much more dramatic with increasing temperature. Hence, at 500 K, the highest T considered, AIMD predicts that the free energy of activation is 9.2 kJ mol^{-1}, i.e., ∼44 % higher compared to that from the static approach.

Table 1: Helmholtz free energies, internal energies, and entropies of activation ($\Delta A^{\ddagger}$, $\Delta U^{\ddagger}$, and $\Delta S^{\ddagger}$, respectively) and of reaction ($\Delta A_{R\to P}$, $\Delta U_{R\to P}$, and $\Delta S_{R\to P}$, respectively) for the transformation of the protonated isobutanol to protonated butan-2-ol (I2), the protonated butan-2-ol to a complex of carbenium cation and water (DH4),and the protonated isobutanol to a complex of carbenium cation and water (DHI) in the gas phase at different temperatures determined using the static approach and AIMD (values in parentheses). The values after the $\pm$ sign represent the standard errors. Note that to make the comparison consistent with the AIMD results, vibrational contributions used in the static approach were determined semi-classically (see Section SIII in Supporting Information for comparison of semi-classical and quantum mechanical results).

Reaction	Quantity	Temperature		
		100 K	300 K	500 K
I2	$\Delta A^{\ddagger}$ (kJ mol^{-1})	43.5 (47.9 $\pm$ 0.1)	31.6 (37.0 $\pm$ 0.2)	20.9 (30.1 $\pm$ 0.2)
	$\Delta U^{\ddagger}$ (kJ mol^{-1})	50.0	48.4	46.7
	$\Delta S^{\ddagger}$ (J mol^{-1} K^{-1})	65.0	55.9	51.6
	$\Delta A_{R\to P}$ (kJ mol^{-1})	-24.5 (-20.5 $\pm$ 0.3)	-24.9 (-22.8 $\pm$ 0.4)	-25.2 (-24.0 $\pm$ 0.5)
	$\Delta U_{R\to P}$ (kJ mol^{-1})	-24.3	-24.3	-24.3
	$\Delta S_{R\to P}$ (J mol^{-1} K^{-1})	1.9	1.9	1.9
DH4	$\Delta A^{\ddagger}$ (kJ mol^{-1})	46.3 (46.6 $\pm$ 0.2)	36.5 (38.8 $\pm$ 0.2)	28.0 (32.5 $\pm$ 0.5)
	$\Delta U^{\ddagger}$ (kJ mol^{-1})	51.6	50.0	48.3
	$\Delta S^{\ddagger}$ (J mol^{-1} K^{-1})	53.9	44.8	40.6
	$\Delta A_{R\to P}$ (kJ mol^{-1})	41.3 (42.1 $\pm$ 0.2)	32.2 (33.0 $\pm$ 0.3)	23.0 (20.5 $\pm$ 0.6)
	$\Delta U_{R\to P}$ (kJ mol^{-1})	45.9	45.9	45.9
	$\Delta S_{R\to P}$ (J mol^{-1} K^{-1})	45.7	45.7	45.7
DHI	$\Delta A^{\ddagger}$ (kJ mol^{-1})	n.a. (48.3 $\pm$ 0.2)	n.a. (38.2 $\pm$ 0.4)	n.a. (31.3 $\pm$ 0.5)
	$\Delta U^{\ddagger}$ (kJ mol^{-1})	n.a.	n.a.	n.a.
	$\Delta A_{R\to P}$ (kJ mol^{-1})	n.a. (24.0 $\pm$ 0.5)	n.a. (10.6 $\pm$ 0.8)	n.a. (-0.3 $\pm$ 1.0)
	$\Delta U_{R\to P}$ (kJ mol^{-1})	n.a.	n.a.	n.a.

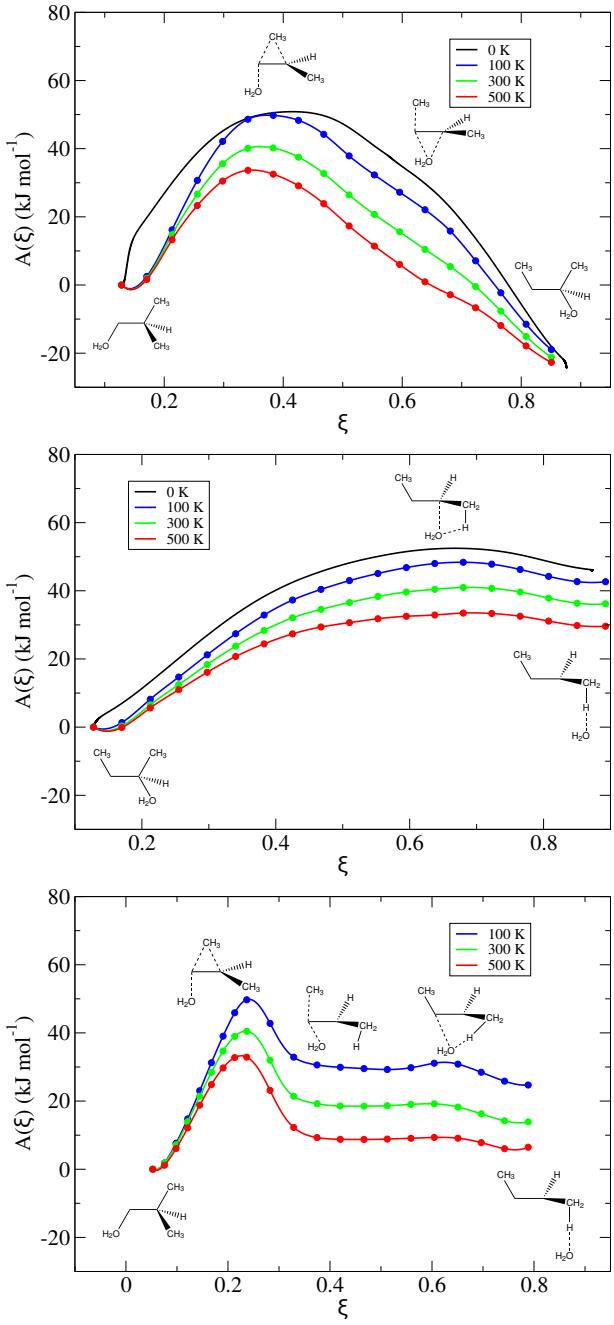

Figure 6: Free energy profiles computed using AIMD for the I2 reaction (top),DH4 reaction (middle), and DHI reaction of protonated isobutanol to carbenium ion (bottom) in the gas phase at 100, 300 and 500 K. The points used in the Blue moon calculations are highlighted by circle symbols. For the sake of comparison, potential energy profile along IRC projected onto ξ (0 K) is also shown for the I2 reaction. All the species depicted on these diagrams hold a +1 charge.

Anharmonicity affects also the structure of the dynamical transition state. Nevertheless, these effects are relatively small, as documented by Figure 5. For instance, the O-C bond that breaks during the reaction shortens systematically with T: from 2.49 Å found in the relaxed structure corresponding to classical 0 K limit, over 2.40 Å at 100 K to 2.32 Å at 500 K. This result indicates that, as a consequence of its higher kinetic energy, H_2O molecule is likely to disconnect from C earlier when T is increased. The evolution of the C-C bond lengths also confirms the earlier TS as T increases (a similar conclusion can be made also by inspecting the free energy profiles shown in Figure 6 that we discuss below). The thermal effect on the bond lengths in reactant and product is only modest, as documented in Figure S21.

Dynamic effects affect the free energy of reaction only moderately, see Table 1. For 100 K, AIMD predicts the value that is 4.0 kJ mol^{-1} higher compared to that from the static approach. The difference in predictions of the approaches gradually reduces with increasing T and eventually reaches 1.2 kJ mol^{-1} at 500 K. This behaviour is not unexpected and follows from the fact that both the reactant and product states are similar in nature and hence a large part of anharmonicity contributions cancels out in the $\Delta A_{R\rightarrow P}$ calculation.

Next, we consider the transformation of protonated butan-2-ol to carbenium-water complex (see Figure 2), for which we succeeded to determine IRC profile (Figure 6 (middle)). Just like in the I2 reaction, carbenium cation and detached water are formed after passing over TS and this type of structures differs from the structures from 'diffuse water' region only in relative position of H_2O with respect to the cation. The corresponding thermodynamic data obtained using the static and AIMD approaches are presented in Table 1. The results follow the trend expected from the nature of TS and product: due to strong entropic stabilization, both the free energy of activation and reaction decrease with temperature. Although the free energies of activation are very similar to those for reaction I2, the reactant of DH4 is $\sim$25 kJ mol^{-1} lower in energy than the reactant of I2. Consequently, the free energies of transition states of DH4 are always significantly lower than those of

TS of I2 reaction. Combining the free energies of reactions for the I2 and DH4 reactions, free energy differences between the product complex and the protonated isobutanol can be determined. The computed values are 22.2, 12.9, and 1.5 kJ mol^{-1} for 100, 300 and 500 K, respectively, and the observed trend can be explained by a large entropic stabilization that results from converting a part of the vibrational degrees of freedom of reactant (most importantly the C-O stretching and C-C-O bending vibrations) into frustrated rotations and translations of separated and only loosely interacting water molecule formed in the product.

3.2 DHI reaction in the gas phase

In our previous work[11] we have shown that, instead of passing through isobutanol to butan-2-ol isomerisation (I2) and the dehydration (DH4), the isobutanol to but-1-ene transformation can occur as a single step reaction (DHI reaction in Figure 1). Here, we shall focus on the gas phase analogue of the DHI reaction, in which, due to the absence of a Brønsted base, in the case of a zeolite catalyst provided by framework O atoms, a complex of neutral water and linear carbenium cation is formed instead of an alkene (see Figure 2 c)).

A direct route from protonated isobutanol and the product complex in the gas phase was not identified in static calculations and, as our AIMD results suggest (*vide infra*), such a direct path containing only one TS probably does not exist at zero temperature. We therefore defined reaction coordinate for our AIMD calculations using the IRC determined in our previous work[11] for the DHI reaction in CHA. Selected snapshots of the structure sampled along ξ are shown in Figure S19. The computed free energy of reaction decreases from 24.0 kJ mol^{-1} at 100 K to -0.3 kJ mol^{-1} at 500 K (see Table 1) and these results are in reasonable agreement with the free energy differences between the water-carbenium cation complex and isobutanol determined when considering the reaction channel consisting of the I2 and DH4 elementary steps (see Section 3.1). A similar

trend is observed also for the computed free energy of activation, which decreases from 48.3 kJ mol^{-1} to 31.3 kJ mol^{-1} as temperature is increased from 100 to 500 K.

A visual inspection of free energy profiles shown in Figure 6 reveals several important trends. Starting from the reactant (protonated isobutanol), a barrier has to be reached (TS close to ξ = 0.23) after which a carbenium cation non-specifically interacting with water molecule is formed as an intermediate. It is a metastable state separated from the final state (complex of water specifically interacting with a C-H bond of carbenium cation) via a small but non-negligible free energy barrier. The presence of this barrier appears to be the reason why our static approach based attempts to identify IRC connecting reactant with product of the gas phase DHI failed. The height of this barrier decreases with T so that it eventually becomes lower than k_BT ($\approx$4 kJ mol^{-1}) at 500 K, which indicates that it can be spontaneously overcome with a great likelihood even during a short AIMD run. The free energy minimum corresponding to the metastable state is broad and shallow because this part of the profile essentially corresponds to diffusive motion of water along carbenium cation. From the chemical point of view, the metastable and the final states correspond to the same system, which is water weakly interacting with carbenium cation. Since the free energy barrier separating the metastable from the final state is negligible compared to the highest barrier on the path between the reactant and product of DHI, considering DHI as a sequence of two elementary steps would have no practical effect on predictions of kinetics of this reaction.

Importantly, the computed values of $\Delta A^{\ddagger}$ for DHI are within 1.2 kJ mol^{-1} identical to that of the I2 reaction. Combined with strong similarity of the averaged structures of dynamical transition states (see Figure 5), these results suggest that both reactions share the same dynamical TS. This hypothesis is supported further by the fact that the distribution of values of reaction coordinate defined for reaction DHI but computed for the free energy TS configurations of I2 are sharply peaked near the value of ξ^* obtained in Blue moon MD simulations of DHI (see Figure 8). Combining the assumption of a common

transition state with the fact that the I2 and DHI mechanisms differ only in the trajectory of water (in I2, water reconnects to a carbon atom, while in DHI it moves away or interacts with H on one of the CH_3 or CH_2 groups, see Figure 7) it becomes clear that the product of transformation will depend on initial conditions at the transition state (specifically, on atomic momenta in the given configuration from the ensemble of TS structures). Hence, for instance, starting from the same configuration selected from ensemble of TS configurations (i.e., structures with $\xi(\boldsymbol{q}) = \xi^*$) initialized with different momenta, different product can be formed. The existence of a common transition state for multiple reactions[34,35] is inconsistent with basic assumptions of transition state theory[62] (TST), which therefore cannot be used to predict the relative importance of the two reactions under different conditions. In particular, the common transition and initial states for two or more reactions imply the same free energies of activation. Since, within the TST, the latter fully determines the rate constants, the kinetics of such competing reaction steps would be identical.

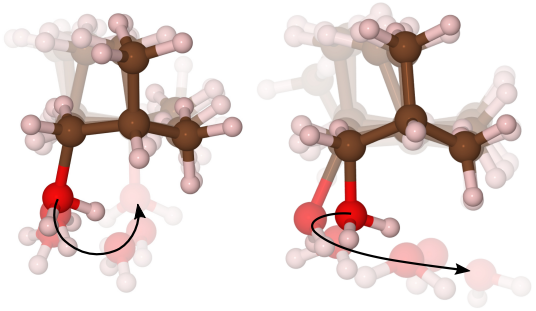

Figure 7: Evolution of atomic positions during the I2 (left) and DHI (right) transformations in gas phase. The reactant state (protonated isobutanol) is represented by an opaque image and the time progress is encoded into a gradually increasing transparency of images obtained as snapshots from constrained AIMD simulations. The arrows indicate the trajectories of water during both transformations.

In the Bennett-Chandler theory,[31,32] the TST rate constant is corrected by multiplying by the transmission coefficient κ, which takes into account the TS recrossings, which is a dynamical effect neglected in TST. The value of the coefficient κ reflects the purely dynam-

ical effects, which cannot be described by a stationary quantity such as the free energy. Hence, within the Bennett-Chandler theory, the relative kinetics of competing reactions with a common TS is determined entirely by the ratio of their respective transmission coefficients. We determined this ratio for the reactions I2 and DHI (here κ_{I2}/κ_{DHI}) as described in Simulation details. To this end, we used ensemble of free energy TS structures obtained in AIMD simulations of the I2 reaction to prepare 5000 different initial conditions (atomic positions and momenta) that were subsequently integrated forward and backward in time and combined together to obtain ensemble of TS-crossing trajectories of total length of 2 ps each. The trajectories were then processed and reactive trajectories, i.e., those with protonated isobutanol at one end and protonated butan-2-ol (for I2) or carbenium cation with water at the other end (for DHI), were identified. At 100 K, 84 % reactive trajectories were found to correspond to reaction I2 and 16 % to DHI. At 500 K, these ratios reversed to 17 % and 83 % for I2 and DHI, respectively. The computed ratios κ_{I2}/κ_{DHI} are 4.4 and 0.2 for T=100 and 500 K, respectively, and these values are close to the ratios of number reactive trajectories corresponding to these mechanisms (84/16=5.3 (100 K) and 17/83=0.2 (500 K)). Thus, we conclude that the dominant reaction mechanism changes from I2 to DHI as temperature is increased. Clearly, this is a consequence of entropic stabilization of the carbenium cation and water pair at high T, obvious also from our free energy data presented in Table 1 .

In order to complement our analysis of transition state crossing trajectories, transition path sampling[33] (TPS) simulations have been conducted for temperatures of 100 and 500 K. The initial trajectory was created by integrating forward and backward in time starting from a relaxed TS structure of the I2 reaction and randomly Maxwell-Boltzmann distributed[63] momenta. As reactive trajectory, the one starting with protonated isobutanol (reactant) and ending with any other form of alcohol or carbenium ion complex (product) with water was considered. The usual shooting move[33] was used to generate trial moves. The length of trajectories was fixed at 500 fs. After performing 2000 trial moves, all the

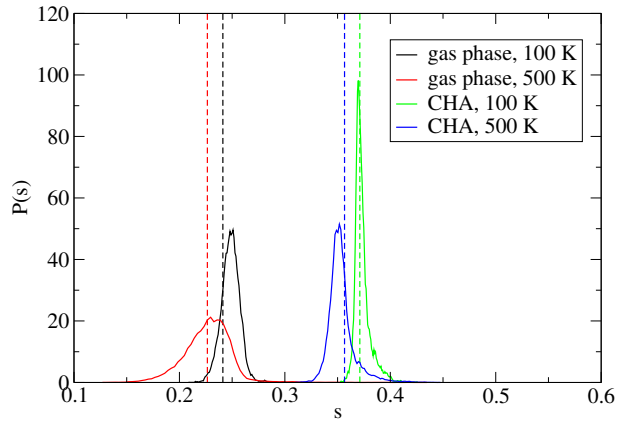

Figure 8: Probability density of coordinate s defined for the DHI reaction in gas phase and CHA computed for the free energy transition state configurations of reaction I2 at 100 and 500 K. The dashed lines indicate the positions of free energy transition states determined in Blue moon calculations of reaction DHI.

accepted trajectories were continued for another 500 fs on the product site and products were automatically identified based on geometric criteria. Carbenium cations with water and butenes with hydroxonium cations were considered as one group of product states, because of the frequent proton jumps between water and carbenium cations that were observed. Out of the reactive trajectories, 94 % led to formation of protonated butan-2-ol, and 6 % to carbenium cation and water at 100 K. At 500 K, protonated butan-2-ol was created in the case of 21 % , while carbenium cation and water in 79 % of reactive trajectories. Hence, the TPS results are in a good qualitative agreement with our barrier crossing analysis.

3.3 Reactions in chabazite

The I2with DH4 and DHI reactions catalyzed by a zeolite differ from the model gas phase reactions discussed previously in Sections 3.1 and 3.2 in two important aspects. First, alcohol molecules formed as reactant and product are not fully protonated. The total charge of atoms of alcohol and proton sitting on zeolite is 0.77 (reactant) or 0.79 $|e|$ (product of I2) but since the charge of the proton is 0.54 $|e|$, the total charge transferred from zeo-

lite to reactant and product alcohol molecules is only 0.23 and 0.25 $|e|$, respectively. As a consequence, the C_4H_9 fragment is less carbocationic than in gas phase (see Figure 4). Since the free energy differences between the neutral butan-2-ol and isobutanol (the values computed using the static approach for T=100 K, 300 K and 500 K are -8.9, -8.8 and -8.6 kJ mol^{-1}, respectively) are very different from those for the protonated systems (see Table 1), these differences in amount of charge transferred can be expected to have a very significant effect on the relative stability of reactant and product and, consequently, also on free energetics of the reaction. Second, all reaction intermediates created during reaction are subject to interaction with zeolite framework, the nature of which tends to change in the course of reaction. In this section we discuss the importance of these effects.

3.3.1 I2 and DH4 reactions

The reaction thermodynamic data for I2 determined using the static and AIMD approaches are collected in Table 2, the corresponding free energy profiles obtained by Blue moon and potential energy profile from IRC are shown in Figure S12 in SI. Just like in the case of the gas phase reaction, the activation barrier decreases with T, namely from 140.9 to 122.6 kJ mol^{-1} (static approach) and from 139.7 to 122.5 kJ mol^{-1} (AIMD) over the temperature range from 100 to 500 K. Thus, the magnitude of thermally induced changes in $\Delta A^{\ddagger}$ is very similar to that in the gas phase, whether static or AIMD approach is considered. This trend results from the nature of reactant and transition state. The reactant corresponds to a relatively stable adsorption complex, in which alcohol is bound to the bridging OH group site via a strong H-bond. Although the H-bond limits the translational and rotational motion of the reactant molecule to some extent, a part of the molecular rotational degrees of freedom are still available. TS is formed in the open space available in the CHA framework, whereby the water molecule remains to be bound to zeolite via hydrogen bonds while the fragment corresponding to carbenium cation is, in contrast to the reactant, not in a direct contact with zeolite (see Figure S22). According to iterative Hirshfeld analy-

sis, the charge of the water - carbenium cation complex formed in TS in CHA is 0.92 $|e|$, which is close to charge 1.00 $|e|$ of TS in vacuum. Interactions with zeolite seem to have only minimal effect on the TS structure, as evident from the close similarity of geometries of TS configurations in vacuum and zeolite (see Figure 5) and from very similar variation of bonds that are broken or formed during the transformation (see Figure 3). Hence, just like in the gas phase TS, nearly neutral water (q=0.08 $|e|$, see Figure 4) is separated from the carbenium cation, giving rise to significant entropy increase. The comparison of temperature dependence of $\Delta A^{\ddagger}$ computed for the reaction in CHA with that in the gas phase suggests that the entropy changes are similar in both cases. Hence the mobility of carbenium cation formed in TS of the CHA catalyzed reaction must be restricted to some extent so that it is similar to that of the H-bonded reactant. A possible explanation for this somewhat surprising finding lies in stabilization of position of cation by Coulombic interactions that cause a rapid increase in energy with distance when charge separation is increased. As shown in Figure S27, the amount of charge transferred to molecule increases in the course of reaction and reaches its maximum close to the relaxed TS. At the same time, the electronic energy monotonously increases with charge and, interestingly, this dependence is very similar for the reactant to TS and for the product to TS parts of the IRC (see Figure 4). The distance between the center of charge of cation and the Al atom (chosen as a reference point as it is approximately symmetrically surrounded by four basic O atoms on which the negative charge is localized) takes the maximum value in TS and hence a farther separation of charge caused by shifting carbenium cation further away from zeolite would indeed cause increase in energy, as observed for other cations in the absence of water.[18] The charge separation in TS is one of the likely reasons, together with degree of protonation of reactant (*vide infra*), for a significant increase (by at least 90 kJ mol^{-1}, see Table 2) in free energy of activation as compared to the reaction in vacuum.

Judging from the static calculations presented in Table 2, free energy of reaction catalyzed by CHA systematically decreases with T. The value computed for 100 K is 8.4 kJ

Table 2: Helmholtz free energies, internal energies, and entropies of activation ($\Delta A^{\ddagger}$, $\Delta U^{\ddagger}$, and $\Delta S^{\ddagger}$, respectively) and of reaction ($\Delta A_{R\to P}$, $\Delta U_{R\to P}$, and $\Delta S_{R\to P}$, respectively) for the transformation of isobutanol to butan-2-ol (I2), butan-2-ol to a but-1-ene (DH4),and isobutanol to but-1-ene (DHI) in CHA at different temperatures determined using the static approach and AIMD (values in parentheses). The values after the $\pm$ sign represent the standard errors. Note that to make the comparison consistent with the AIMD results, vibrational contributions were determined semi-classically (see Section SIII in Supporting Information for comparison of semi-classical and quantum mechanical results).

Reaction	Quantity	Temperature		
		100 K	300 K	500 K
I2	$\Delta A^{\ddagger}$ (kJ mol^{-1})	140.9 (139.7 $\pm$ 0.3)	131.1 (129.6 $\pm$ 0.5)	122.6 (122.5 $\pm$ 0.6)
	$\Delta U^{\ddagger}$ (kJ mol^{-1})	146.3	144.6	143.0
	$\Delta S^{\ddagger}$ (J mol^{-1} K^{-1})	54.2	45.0	40.8
	$\Delta A_{R\to P}$ (kJ mol^{-1})	-16.1 (-12.4 $\pm$ 0.5)	-20.8 (-5.8 $\pm$ 0.8)	-25.4 (-4.5 $\pm$ 1.0)
	$\Delta U_{R\to P}$ (kJ mol^{-1})	-13.7	-13.7	-13.7
	$\Delta S_{R\to P}$ (J mol^{-1} K^{-1})	23.4	23.4	23.4
DH4	$\Delta A^{\ddagger}$ (kJ mol^{-1})	116.6 (115.0 $\pm$ 0.3)	108.3 (106.8 $\pm$ 0.4)	101.2 (96.3 $\pm$0.6)
	$\Delta U^{\ddagger}$ (kJ mol^{-1})	121.3	119.7	118.0
	$\Delta S^{\ddagger}$ (J mol^{-1} K^{-1})	47.0	37.9	33.6
	$\Delta A_{R\to P}$ (kJ mol^{-1})	76.3 (80.5 $\pm$ 0.3)	60.3 (67.7 $\pm$ 0.5)	44.3 (54.7 $\pm$ 0.7)
	$\Delta U_{R\to P}$ (kJ mol^{-1})	84.2	84.2	84.2
	$\Delta S_{R\to P}$ (J mol^{-1} K^{-1})	79.8	79.8	79.8
DHI	$\Delta A^{\ddagger}$ (kJ mol^{-1})	156.8 (143.0 $\pm$ 0.4)	148.3 (125.4 $\pm$ 0.6)	141.2 (121.7 $\pm$ 0.9)
	$\Delta U^{\ddagger}$ (kJ mol^{-1})	161.5	159.8	158.2
	$\Delta S^{\ddagger}$ (J mol^{-1} K^{-1})	47.4	38.3	34.0
	$\Delta A_{R\to P}$ (kJ mol^{-1})	44.0	29.7	15.4
	$\Delta U_{R\to P}$ (kJ mol^{-1})	51.2	51.2	51.2
	$\Delta S_{R\to P}$ (J mol^{-1} K^{-1})	71.5	71.5	71.5

mol^{-1} higher compared to that in the gas phase. This difference, however, reduces with T and the value for reaction in CHA is virtually identical to that in the gas phase at 500 K. The AIMD results for reaction in CHA are, however, significantly different from both the static and gas phase AIMD values. In particular, the values of $\Delta A_{R\to P}$, ranging between -12.4 K (100 K) to -4.5 (500 K) are significantly higher than those determined using the static approach for CHA (-16.1 (100 K) to -25.4 (500 K)) or AIMD for the gas phase reaction (-20.5 (100 K) to -24.0 (500 K)). In fact, the AIMD results are closer to free energy differences between neutral gas phase isobutanol and butan-2-ol molecules (-8.9, -8.8,

and -8.6 kJ mol^{-1} for 100, 300, and 500 K, respectively). To this end, it is useful to analyze the protonation probability (see Figure S23), which we define as $p_{H^+} = N_{H^+}/N_{tot}$, where N_{tot} is the total number of configurations generated in an unconstrained MD run of reactant or product and N_{H^+} is the number of configurations with the distance between the proton and O from alcohol being shorter than that between the proton and basic O on zeolite. For isobutanol, the computed p_{H^+} values are 4.5 %, 22.0 %, and 18.7 % for 100, 300, and 500 K, respectively, while the corresponding values determined for butan-2-ol are 43.1 %, 31.9 %, and 26.2 %. Hence, the protonation probabilities tend to decrease with T, with the anomalous value found for isobutanol at 100 K being the only exception from this trend. Furthermore, the values determined for isobutanol are significantly lower than those for butan-2-ol, which is consistent with lower partial charge determined for the former (*vide supra*). Since a significant part of charge is shifted to C_4H_9 fragment upon protonation (see Figure 4), this result, indicating that butan-2-ol is a stronger Brønsted base, can be explained by lower stability of primary cation, formed in the case of isobutanol, compared to the secondary one, formed in the case of butan-2-ol. As discussed above, the lower degree of protonation leads to increase in the free energy barriers. The different thermally dependent p_{H^+} of reactant and product molecules thus imply a larger increase of the forward barrier and hence a relative stabilization of reactant with respect to product as compared to the gas phase reaction. This is likely the effect affecting the trend in $\Delta A_{R\to P}$ vs. T dependence reported in Table 2. The changes in dispersion interactions in the course of transformation are found to contribute only marginally (less than 3.8 kJ mol^{-1}) to computed $\Delta A^{\ddagger}$ and $\Delta A_{R\to P}$ values.

Just like in the case of the gas phase reactions, we consider the DH4 reaction as an elementary step that succeeds I2 to complete transformation from isobutanol to linear but-1-ene (see Figure S18). In this zeolite-catalyzed reaction, the product forms π complex with the Brønsted site restored during the reaction. As it follows from the computed data compiled in Table 2, the activation free energy of DH4 is at all temperatures at least 20 kJ

mol^{-1} lower compared to that for I2. More importantly, since the I2 reaction is exergonic (*vide infra*), the position of the TS of DH4 on the free energy landscape is more than 30 kJ mol^{-1} below that of TS for I2. From these results we deduce that the contribution of the DH4 step to the kinetics of the I2+DH4 sequence will be unimportant. The DH4 step is strongly endergonic, with $\Delta A_{R\rightarrow P}$ decreasing with T (from 80.5 (100 K) to 54.7 kJ mol^{-1} (500 K)). Combined with the $\Delta A_{R\rightarrow P}$ values for I2 we find that the complex of but-1-ene in zeolite is 50.2 to 68.1 kJ mol^{-1} higher in free energy than isobutanol adsorbed in zeolite, whereby the difference decreases with T. As obvious from the data presented in Table 2, the results obtained using the static approach are in surprisingly good agreement with the AIMD data, with the largest difference found for $\Delta A_{R\rightarrow P}$ at high T, in which case the static approach seems to overestimate the thermal effect.

3.3.2 DHI reaction

The computed thermodynamic properties for the DHI reaction are collected in Table 2. According to the static approach, the free energy barrier is significantly higher than that obtained for the reaction I2, with differences increasing with T, from 15.9 (100 K) to 18.6 kJ mol^{-1} (500 K). However, as evident from Figure 3, the variation of bonds that are broken or formed during the transformation along IRC follow, up to TS, very similar trends as those for the I2 reaction in CHA or in gas phase, suggesting a close similarity of the initial parts of these reactions. The trend in computed free energy of reaction, which decreases from 44.0 at 100 K to 15.4 kJ mol^{-1} at 500 K, approximately reflects temperature dependence of relative stability of isobutanol and but-1-ene in the gas phase (46.1 (100 K), 13.7 (300 K), -16.1 kJ mol^{-1} (500 K)). The AIMD simulations of the DHI reactions are highly problematic because of numerous possible side reactions occurring upon crossing TS, which are difficult to avoid without drastically biasing the sampling. Deprotonation of carbenium, for instance, can involve any of its H atoms located on its CH_3 and CH_2 groups, whereby the proton can be transferred to any O atom of zeolite neighboring Al,

and the process can be assisted by water molecule whose location is also difficult to control, due to its relatively weak H-bonding interactions with zeolite. Therefore, we were not able to reliably determine $\Delta A_{R\rightarrow P}$ and decided to focus here only on the free energy of activation. We note however, that $\Delta A_{R\rightarrow P}$ corresponding to formation of but-1-ene, which is one of the possible products of the DHI reaction, the corresponding $\Delta A_{R\rightarrow P}$ must be identical to the free energy difference between isobutanol and but-1-ene determined in our calculations of the I2+DH4 sequence. Free energy profiles obtained by Blue moon and potential energy profile from IRC are shown in Figure S15. According to our calculations, the AIMD results for $\Delta A^{\ddagger}$ are at all temperatures significantly lower compared to the static results and, in analogy to the gas phase reactions, they are very similar (within 4.2 kJ mol^{-1} - note that these small differences are likely due to systematic error in free energy calculations caused, e.g., by the numerical scheme used in free energy gradients integrations, or by the use of imperfect approximation for the (unknown) reaction coordinate) to the values obtained for the reactions I2 (see Table 2). Since also the geometries of dynamic transition states appear to be very close to those of the I2 reaction (see Figure 5), it is reasonable to assume that, just like in the gas phase, both reactions share a common TS (see Figure 8).

In order to determine relative importance of both reactions, we used the simulation protocol described in Section 3.2 to generate an ensemble of TS-crossing trajectories. At 100 K, 80 % of reactive trajectories corresponded to reaction I2 and 20 % to DHI reaction, while the corresponding ratio of transmission coefficients (in the case of common TS corresponding also to ratio of rate constants) is $\sim$3.7. Compared to the gas phase for which $\kappa_{I2}/\kappa_{DHI} \approx 4.4$ was predicted, the relative frequency of the I2 reaction is therefore slightly reduced. Just like in the gas phase, the percentage of the reactive trajectories corresponding to I2 is reduced with increasing T, but the change is less significant than in the gas phase. At 500 K, 55 % reactive trajectories were found to correspond to I2 and 45 % to DHI, while $\kappa_{I2}/\kappa_{DHI} \approx$1.3. Thus, even though the I2 reaction still remains domi-

nant, the alternative reaction channel occurs with nearly the same frequency (a situation summarized in Figure 9). In contrast, the data obtained from the static approach suggest a radically different picture: the ratio of rate constants is estimated to be $\sim 20.10^7$ at 100 K and $\sim$88 at 500 K. Finally, note that the computed selectivities seem to correlate with the heights of the free energy barriers of I2 and DHI reactions shown in Table 2. However, since all the trajectories used in the κ calculations were initialized from the TS for I2 (and hence all trajectories were guaranteed to pass through the TS for I2), such a correlation should be viewed as coincidental. This is well evident in the case of the gas phase reactions (Table 1), where the differences in free energy barriers are very small and uncorrelated with the observed T-dependence of selectivity. Specifically, the barrier for I2 at 500 K in gas phase is 1.2 kJ mol^{-1} lower than that for the DHI (which should indicate selectivity towards I2), yet the computed transmission coefficient of I2 is factor 5 lower than that for DHI.

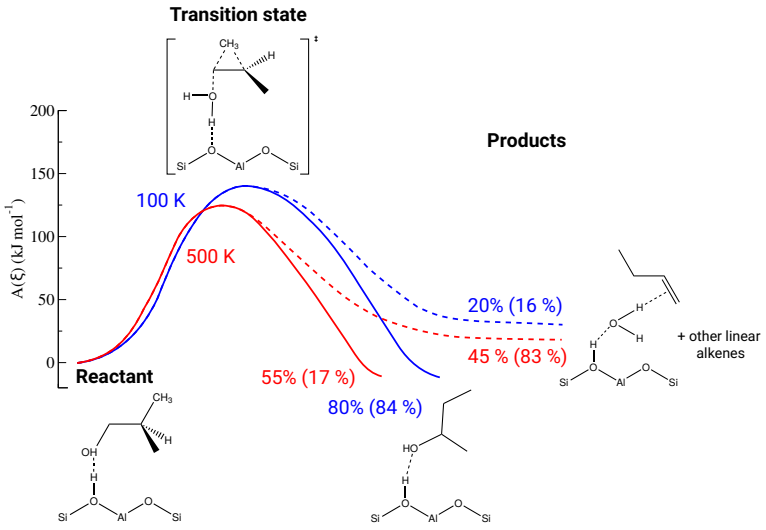

Figure 9: Relative frequency of I2 and DHI reaction mechanisms passing through common TS in CHA and in gas phase (values in parentheses) at 100 (blue) and 500 K (red).

4 Conclusions

In this work, theoretical investigation of isobutanol isomerization and synchronous isomerization and dehydration reactions catalyzed by acid zeolite, identified in our previous work[11] as the key steps in whole network of transformations linking isobutanol with butenes, has been conducted by means of AIMD simulations. Using gas phase model reactions, it has been demonstrated that the isomerization of isobutanol into butan-2-ol (called I2) and the synchronous dehydration and isomerization of isobutanol into linear butenes (DHI) reactions share a common dynamical transition state. Consequently, the relative reaction rates of these two competing reactions is given by the ratio of their respective transmission coefficients. The latter depends sensitively on the thermodynamic conditions. Temperature favours the pathway leading to the higher entropy product, which is, in this case, a carbenium loosely interacting with water created in DHI. Thus, switching from 100 to 500 K, the dominant mechanism changes from I2 (yielding butan-2-ol, a product with similar entropy as reactant) to DHI, whereby the estimated κ_{I2}/κ_{DHI} shifts from 4.4 to 0.2. The activation free energy of both gas phase reactions was found to decrease with T from $\sim$48 to $\sim$30 kJ mol^{-1} as T is increased from 100 to 500 K.

The effect of the zeolite catalyst on the I2 and DHI reactions has then been studied using the acid chabazite model. As evident from the geometry of the adsorption complexes and the low charge transferred from zeolite to molecule, both the reactant and the product of the I2 reaction are nearly neutral molecules. This was shown to have a large effect on their relative stabilities which differ significantly from those determined for the reaction in the gas phase, where all intermediates have a charge of 1.0 $|e|$. In the transition state of the reaction catalyzed by zeolite, on the other hand, almost full charge transfer takes place and hence this state is very similar to that in the gas phase. This is a very important effect leading to increase in free energy of activation by $\sim$90 kJ mol^{-1} as compared to the gas phase reaction. Hence, the level of protonation, is identified as a key factor leading to drastic changes in free energetics of the I2 reaction.

Based on a naive comparison of the profiles of the gas phase reactions and reactions catalyzed by zeolite, one may come to incorrect conclusion that zeolites are not optimal catalysts. The important point to realize is that the low barriers computed for the gas phase reaction are due to the very low stability of the protonated reactant, whereas the adsorption complex formed by isobutanol in zeolite is much more stable. This initial stability is needed to start catalysis since the molecule can only be transformed in the zeolite if it is adsorbed. Nevertheless, it is clear that the barriers of isobutanol transformation reactions in the zeolite can be reduced either via decreasing the stability of adsorbed alcohols, while still keeping the molecule adsorbed (i.e., targeting at a free adsorption energy close to zero), or stabilizing the transition states by specific interactions with zeolite, which can be affected by factors such as the choice of the zeolite framework, the Si/Al ratio, location of acid sites. Investigation of this important problem is out of the scope of the present work as it will require a systematic long-term research effort.

Compared to the static approach, the AIMD calculations predict systematically higher free energy barriers and free energies of reaction for the gas phase I2 reaction. The static approach, however, cannot be used to investigate the DHI reaction in the gas phase, since its reactant and product are not connected via zero temperature potential energy path involving only one TS. In the case of I2 reaction in CHA, the static and AIMD approaches yield surprisingly similar results for free energy of activation, but they differ significantly in predictions for the free energy of reaction. This difference increases with T and is caused by the fact that the static approach cannot take into account significant temperature dependent changes in protonation degree of reactant and product molecules. An even more serious flaw in the static approach is the strong overestimation of the free energy barrier for the DHI reaction. Similar to the gas phase, the I2 and DHI reactions in chabazite were found to share a common transition state. The values of κ_{I2}/κ_{DHI} of 3.7 and 1.3 computed at 100 K and 500 K, respectively, indicate qualitatively similar trend as in the gas phase, although the I2 reaction is predicted to occur at slightly greater frequency

than its alternative even at the highest temperature considered. These results represent a significant change compared to the static approach, according to which the ratios of the rate constants of I2 and DHI are $\sim 20.10^7$ and ~ 88 for 100 and 500 K, respectively. Thus, importantly, our results offer a revised view on the relevant reactions at the origin of the formation of linear butenes starting from isobutanol: both isomerization of isobutanol into butan-2-ol and synchronous isomerization and dehydration significantly contribute to the formation of linear butenes starting from isobutanol. This work opens the route to a more precise evaluation of respective rates of reactions and highlights importance of including dynamical effects in the cases, where it is crucial to predict reaction selectivities accurately.

Supporting Information Available

Chabazite supercell, additional information about AIMD free energy calculations, comparison of semi-classical and quantum mechanical harmonic approximation, structural changes along IRC for DHI in CHA, additional figures (PDF)

Acknowledgement

MG and TB acknowledge support from IFP Energies nouvelles within the project "Ab initio Molecular Dynamics Investigation of the Reactivity of Zeolites" , from the Slovak Research and Development Agency under the contract No. APVV-20-0127 and the grant VEGA 1/0254/24 from the Ministry of Education Research, Development and Youth of the Slovak Republic. PR and CC acknowledge the Agence Nationale de la Recherche under France 2030 (contract ANR-22-PEBB-0009), for support in the context of the MAM-ABIO project (B-BEST PEPR). The research was realized using the computational resources procured in the national project National competence centre for high performance

computing within the Operational programme Integrated infrastructure (project code: 311070AKF2).

Author information

Corresponding authors

Tomáš Bučko - Department of Physical and Theoretical Chemistry, Faculty of Natural Sciences, Comenius University in Bratislava, Mlynská Dolina, SK-84215 Bratislava, SLOVAKIA, Institute of Inorganic Chemistry, Slovak Academy of Sciences, Dúbravska cesta 9, SK-84236 Bratislava, SLOVAKIA; orcid.org/0000-0002-5847-9478; tomas.bucko@uniba.sk

Céline Chizallet - IFP Energies nouvelles, Rond-Point de l'Echangeur de Solaize, BP3, 63960, Solaize, FRANCE; orcid.org/0000-0001-5140-8397; celine.chizallet@ifpen.fr

Authors

Monika Gešvandtnerová - Department of Physical and Theoretical Chemistry, Faculty of Natural Sciences, Comenius University in Bratislava, Mlynská Dolina, SK-84215 Bratislava, SLOVAKIA; orcid.org/0000-0001-5561-1755

Pascal Raybaud - IFP Energies nouvelles, Rond-Point de l'Echangeur de Solaize, BP3, 63960, Solaize, FRANCE; orcid.org/0000-0003-4506-5062

References

(1) Atsumi, S.; Hanai, T.; Liao, J. C. Non-fermentative pathways for synthesis of branched-chain higher alcohols as biofuels. *Nature* **2008**, *451*, 86–89.

(2) Buniazet, Z.; Cabiac, A.; Maury, S.; Bianchi, D.; Loridant, S. Unexpected selectivity of ferrierite for the conversion of isobutanol to linear butenes and water effects. *Appl. Catal. B.* **2019**, *243*, 594–603.

(3) Van Daele, S.; Minoux, D.; Nesterenko, N.; Maury, S.; Coupard, V.; Valtchev, V.; Travert, A.; Gilson, J.-P. A highly selective FER-based catalyst to produce n-butenes from isobutanol. *Appl. Catal. B.* **2021**, *284*, 119699.

(4) Savage, N. Fuel options: The ideal biofuel. *Nature* **2011**, *474*, S9–11.

(5) de Reviere, A.; Gunst, D.; Sabbe, M. K.; Reyniers, M.-F.; Verberckmoes, A. Dehydration of butanol towards butenes over MFI, FAU and MOR: influence of zeolite topology. *Catal. Sci. Technol.* **2021**, *11*, 2540–2559.

(6) Domokos, L.; Lefferts, L.; Seshan, K.; Lercher, J. Isomerization of Linear Butenes to iso-Butene over Medium Pore Zeolites: I. Kinetic Aspects of the Reaction over H-FER. *J. Catal.* **2001**, *197*, 68–80.

(7) Liu, W.; Hu, H.; Liu, Y.; Zhang, L.; Xia, C.; Wang, Q.; Ke, M. Distribution of Effective Ferrierite Active Sites for Skeletal Isomerization of n-Butene to Isobutene. *ChemistrySelect* **2019**, *4*, 7851–7857.

(8) Mooiweer, H.; de Jong, K.; Kraushaar-Czarnetzki, B.; Stork, W.; Krutzen, B. In *Zeolites and Related Microporous Materials: State of the Art 1994 - Proceedings of the 10th International Zeolite Conference, Garmisch-Partenkirchen, Germany, 17-22 July 1994*; Weitkamp, J., Karge, H., Pfeifer, H., Hölderich, W., Eds.; Elsevier, 1994; Vol. 84; pp 2327–2334.

(9) Mériaudeau, P.; Tuan, V.; Le, N.; Szabo, G. Selective Isomerization ofn-Butene into Isobutene over Deactivated H–Ferrierite Catalyst: Further Investigations. *J. Catal.* **1997**, *169*, 397–399.

(10) Chizallet, C.; Bouchy, C.; Larmier, K.; Pirngruber, G. Molecular Views on Mechanisms of Brønsted Acid-Catalyzed Reactions in Zeolites. *Chem. Rev.* **2023**, *123*, 6107–6196.

(11) Gešvandtnerová, M.; Bučko, T.; Raybaud, P.; Chizallet, C. Monomolecular mechanisms of isobutanol conversion to butenes catalyzed by acidic zeolites: Alcohol isomerization as a key to the production of linear butenes. *J. Catal.* **2022**, *413*, 786–802.

(12) John, M.; Alexopoulos, K.; Reyniers, M.-F.; Marin, G. B. Reaction path analysis for 1-butanol dehydration in H-ZSM-5 zeolite: Ab initio and microkinetic modeling. *J. Catal.* **2015**, *330*, 28–45.

(13) John, M.; Alexopoulos, K.; Reyniers, M.-F.; Marin, G. B. First-Principles Kinetic Study on the Effect of the Zeolite Framework on 1-Butanol Dehydration. *ACS Catal.* **2016**, *6*, 4081–4094.

(14) John, M.; Alexopoulos, K.; Reyniers, M.-F.; Marin, G. B. Mechanistic insights into the formation of butene isomers from 1-butanol in H-ZSM-5: DFT based microkinetic modelling. *Catal. Sci. Technol.* **2017**, *7*, 1055–1072.

(15) John, M.; Alexopoulos, K.; Reyniers, M.-F.; Marin, G. B. Effect of zeolite confinement on the conversion of 1-butanol to butene isomers: mechanistic insights from DFT based microkinetic modelling. *Catal. Sci. Technol.* **2017**, *7*, 2978–2997.

(16) Kozuch, S.; Shaik, S. How to Conceptualize Catalytic Cycles? The Energetic Span Model. *Acc. Chem. Res.* **2011**, *44*, 101–110.

(17) Amatore, C.; Jutand, A. Mechanistic and kinetic studies of palladium catalytic systems. *J. Organomet. Chem.* **1999**, *576*, 254–278.

(18) Rey, J.; Gomez, A.; Raybaud, P.; Chizallet, C.; Bučko, T. On the origin of the difference between type A and type B skeletal isomerization of alkenes catalyzed by zeolites: The crucial input of ab initio molecular dynamics. *J. Catal.* **2019**, *373*, 361–373.

(19) Bučko, T.; Benco, L.; Hafner, J.; Ángyán, J. G. Monomolecular cracking of propane over acidic chabazite: An ab initio molecular dynamics and transition path sampling study. *J. Catal.* **2011**, *279*, 220–228.

(20) Cnudde, P.; De Wispelaere, K.; Vanduyfhuys, L.; Demuynck, R.; Van der Mynsbrugge, J.; Waroquier, M.; Van Speybroeck, V. How Chain Length and Branching Influence the Alkene Cracking Reactivity on H-ZSM-5. *ACS Catal.* **2018**, *8*, 9579–9595.

(21) Van Speybroeck, V.; De Wispelaere, K.; Van der Mynsbrugge, J.; Vandichel, M.; Hemelsoet, K.; Waroquier, M. First principle chemical kinetics in zeolites: the methanol-to-olefin process as a case study. *Chem. Soc. Rev.* **2014**, *43*, 7326–7357.

(22) Rey, J.; Bignaud, C.; Raybaud, P.; Bučko, T.; Chizallet, C. Dynamic Features of Transition States for β-Scission Reactions of Alkenes over Acid Zeolites Revealed by AIMD Simulations. *Angew. Chem. Int. Ed.* **2020**, *59*, 18938–18942.

(23) Bocus, M.; Vanduyfhuys, L.; De Proft, F.; Weckhuysen, B. M.; Van Speybroeck, V. Mechanistic Characterization of Zeolite-Catalyzed Aromatic Electrophilic Substitution at Realistic Operating Conditions. *JACS Au* **2022**, *2*, 502–514.

(24) Laio, A.; Parrinello, M. Escaping free-energy minima. *Proc. Natl. Acad. Sci. U.S.A.* **2002**, *99*, 12562.

(25) Torrie, G. M.; Valleau, J. P. Nonphysical sampling distributions in Monte Carlo free-energy estimation: Umbrella sampling. *J. Comput. Phys.* **1977**, *23*, 187–199.

(26) Carter, E.; Ciccotti, G.; Hynes, J. T.; Kapral, R. Constrained reaction coordinate dynamics for the simulation of rare events. *Chem. Phys. Lett.* **1989**, *156*, 472 – 477.

(27) Sprik, M.; Ciccotti, G. Free energy from constrained molecular dynamics. *J. Chem. Phys.* **1998**, *109*, 7737–7744.

(28) Cnudde, P.; De Wispelaere, K.; Van der Mynsbrugge, J. Effect of temperature and branching on the nature and stability of alkene cracking intermediates in H-ZSM-5. *J. Catal.* **2017**, *345*, 53–69.

(29) Hill, T. *Free Energy Transduction in Biology: The steady-State Kinetic and Thermodynamic Formalism*; Elsevier, 2012.

(30) Pigeon, T.; Stoltz, G.; Corral-Valero, M.; Anciaux-Sedrakian, A.; Moreaud, M.; Lelièvre, T.; Raybaud, P. Computing Surface Reaction Rates by Adaptive Multilevel Splitting Combined with Machine Learning and Ab Initio Molecular Dynamics. *J. Chem. Theory Comput.* **2023**, *19*, 3538–3550.

(31) Bennett, C. H. *Algorithms for Chemical Computations*; Chapter 4, pp 63–97.

(32) Chandler, D. Statistical mechanics of isomerization dynamics in liquids and the transition state approximation. *J. Chem. Phys.* **1978**, *68*, 2959–2970.

(33) Dellago, C.; Bolhuis, P. G.; Chandler, D. Efficient transition path sampling: Application to Lennard-Jones cluster rearrangements. *J. Chem. Phys.* **1998**, *108*, 9236–9245.

(34) Ess, D. H.; Wheeler, S. E.; Iafe, R. G.; Xu, L.; Çelebi Ölçüm, N.; Houk, K. N. Bifurcations on Potential Energy Surfaces of Organic Reactions. *Angew. Chem., Int. Ed.* **2008**, *47*, 7592–7601.

(35) Hare, S. R.; Tantillo, D. J. Post-transition state bifurcations gain momentum – current state of the field. *Pure Appl. Chem.* **2017**, *89*, 679–698.

(36) Nieves-Quinones, Y.; Singleton, D. A. Dynamics and the Regiochemistry of Nitration of Toluene. *J. Am. Chem. Soc.* **2016**, *138*, 15167–15176.

(37) Hong, Y. J.; Tantillo, D. J. Biosynthetic consequences of multiple sequential post-transition-state bifurcations. *Nature Chem.* **2014**, *6*, 104–111.

(38) Xue, X.-S.; Jamieson, C. S.; Garcia-Borràs, M.; Dong, X.; Yang, Z.; Houk, K. N. Ambimodal Trispericyclic Transition State and Dynamic Control of Periselectivity. *J. Am. Chem. Soc.* **2019**, *141*, 1217–1221.

(39) Pu, M.; Nielsen, C. D.-T.; Senol, E.; Sperger, T.; Schoenebeck, F. Post-Transition-State Dynamic Effects in the Transmetalation of Pd(II)-F to Pd(II)-CF3. *JACS Au* **2024**, *4*, 263–275.

(40) Kresse, G.; Hafner, J. Ab initio molecular dynamics for liquid metals. *Phys. Rev. B* **1993**, *47*, 558–561.

(41) Kresse, G.; Hafner, J. Ab-Initio Molecular-Dynamics Simulation of the Liquid-Metal Amorphous-Semiconductor Transition in Germanium. *Phys. Rev. B* **1994**, *49*, 14251–14269.

(42) Kresse, G.; Furthmuller, J. Efficient iterative schemes for ab initio total-energy calculations using a plane-wave basis set. *Phys. Rev. B* **1996**, *54*, 11169–11186.

(43) Blochl, P. E. Projector Augmented-Wave Method. *Phys. Rev. B* **1994**, *50*, 17953–17979.

(44) Kresse, G.; Joubert, D. From ultrasoft pseudopotentials to the projector augmented-wave method. *Phys. Rev. B* **1999**, *59*, 1758–1775.

(45) Perdew, J. P.; Burke, K.; Ernzerhof, M. Generalized gradient approximation made simple. *Phys. Rev. Lett.* **1996**, *77*, 3865–3868.

(46) Grimme, S. Semiempirical GGA-type density functional constructed with a long-range dispersion correction. *J. Comput. Chem.* **2006**, *27*, 1787–1799.

(47) Bučko, T.; Hafner, J.; Lebégue, S.; Ángyán, J. G. Improved Description of the Structure of Molecular and Layered Crystals: Ab Initio DFT Calculations with van der Waals Corrections. *J. Phys. Chem. A* **2010**, *114*, 11814–11824.

(48) Bultinck, P.; Van Alsenoy, C.; Ayers, P. W.; Carbó Dorca, R. Critical analysis and extension of the Hirshfeld atoms in molecules. *J. Chem. Phys.* **2007**, *126*, 144111.

(49) Bučko, T.; Lebegue, S.; Hafner, J.; Angyán, J. G. Improved density dependent correction for the description of London dispersion forces. *J. Chem. Theory Comput.* **2013**, *9*, 4293–4299.

(50) Smith, L.; Davidson, A.; Cheetham, A. K. A neutron diffraction and infrared spectroscopy study of the acid form of the aluminosilicate zeolite, chabazite (H- SSZ-13). *Catal. Letters* **1997**, *49*, 143–146.

(51) Frenkel, D.; Smit, B. In *Understanding Molecular Simulation (Second Edition)*, second edition ed.; Frenkel, D., Smit, B., Eds.; Academic Press: San Diego, 2002.

(52) Nosé, S. A unified formulation of the constant temperature molecular-dynamics methods. *J. Chem. Phys.* **1984**, *81*, 511.

(53) Hoover, W. Canonical dynamics - Equilibrium phase-space distributions. *Phys. Rev. A* **1985**, *31*, 1695.

(54) Verlet, L. Computer "Experiments" on Classical Fluids. I. Thermodynamical Properties of Lennard-Jones Molecules. *Phys. Rev.* **1967**, *159*, 98–103.

(55) Schiferl, S. K.; Wallace, D. C. Statistical errors in molecular dynamics averages. *J. Chem. Phys.* **1985**, *83*, 5203–5209.

(56) Bučko, T.; Chibani, S.; Paul, J.-F.; Cantrel, L.; Badawi, M. Dissociative iodomethane adsorption on Ag-MOR and the formation of AgI clusters: an ab initio molecular dynamics study. *Phys. Chem. Chem. Phys.* **2017**, *19*, 27530–27543.

(57) Bučko, T.; Hafner, J. The role of spatial constraints and entropy in the adsorption and transformation of hydrocarbons catalyzed by zeolites. *J. Catal.* **2015**, *329*, 32–48.

(58) Branduardi, D.; Gervasio, F. L.; Parrinello, M. From A to B in free energy space. *J. Chem. Phys.* **2007**, *126*, 054103.

(59) Hratchian, H. P.; Schlegel, H. B. Following Reaction Pathways Using a Damped Classical Trajectory Algorithm. *J. Phys. Chem. A* **2002**, *106*, 165–169.

(60) Zwanzig, R. W. High-Temperature Equation of State by a Perturbation Method. I. Nonpolar Gases. *J. Chem. Phys.* **1954**, *22*, 1420–1426.

(61) Bučko, T.; Gešvandtnerová, M.; Rocca, D. Ab Initio Free Energy Calculations at Multiple Electronic Structure Levels Made Affordable: An Effective Combination of Perturbation Theory and Machine Learning. *J. Chem. Theory Comput.* **2020**, *16*, 6049–6060.

(62) Eyring, H. The activated complex in chemical reactions. *J. Chem. Phys.* **1935**, *3*, 107–115.

(63) Tuckerman, M. E. *Statistical Mechanics: Theory and Molecular Simulation*; Oxford University Press, 2010.

TOC Graphic